J|A|C|S ARTICLES

Published on Web 10/15/2009

Single-Ion Reorganization Free Energy of Aqueous $Ru(bpy)_3^{2+/3+}$ and $Ru(H_2O)_6^{2+/3+}$ from Photoemission Spectroscopy and Density Functional Molecular Dynamics Simulation

Robert Seidel,[†] Manfred Faubel,[‡] Bernd Winter,[†] and Jochen Blumberger*[,§]

Helmholtz-Zentrum Berlin für Materialien und Energie, and BESSY, Albert-Einstein-Strasse 15, D-12489 Berlin, Germany, Max-Planck-Institut für Dynamik and Selbstorganisation, Bunsenstrasse 10, D-37073 Göttingen, Germany, and Department of Chemistry, University of Cambridge, Lensfield Road, Cambridge CB2 1EW, U.K.

Received June 11, 2009; E-mail: bernd.winter@bessy.de; jb376@cam.ac.uk

Abstract: Photoelectron spectroscopy and density functional molecular dynamics simulations are combined to quantify and characterize the redox properties of $Ru(bpy)_3^{2+/3+}$ and $Ru(H_2O)_6^{2+/3+}$ in aqueous solution. We report the energy-resolved photoelectron spectrum of aqueous $Ru(bpy)_3^{2+}$ at 200 eV photon energy. From the peak position of the highest molecular orbital at 6.81 eV, an experimental value for the single-ion reorganization free energy of $Ru(bpy)_3^{3+}$ is determined to be 1.21 ± 0.04 eV. Density functional molecular dynamics calculations give a value of 0.84−1.20 eV for $Ru(bpy)_3^{3+}$ and 1.92−2.42 eV for $Ru(H_2O)_6^{3+}$ depending on the method used to extrapolate the results to the infinite dilution limit. Since linear response is an excellent approximation for these systems, we report the same reorganization free energies for the divalent ions. The relatively small reorganization free energy of $Ru(bpy)_3^{3+}$ is a consequence of the small changes in the Ru−N bond lengths upon reduction (0.04 eV inner sphere contribution) and of the large hydrophobic cavity formed by the bulky bipyridine ligands, which effectively reduces the dipolar response of the solvent in qualitative agreement with continuum theory. The large difference in redox potential between $Ru(bpy)_3^{2+/3+}$ and $Ru(H_2O)_6^{2+/3+}$ (1 eV) is mainly associated with the difference in reorganization free energy rather than vertical ionization energy. Finally, the measured photoelectron spectrum of $Ru(bpy)_3^{2+}$ is compared with the Kohn−Sham density of states for interpretation of occupied as well as computed virtual energy levels. This computational approach, in conjunction with first-ever photoelectron spectroscopy measurements of an aqueous transition metal ion, provides a quantitative benchmark for understanding the effect of water on metal redox potential and lays the groundwork for future studies of redox properties.

1. Introduction

The influence of the ligand on the redox properties of a transition metal ion can be substantial. For instance, the reduction potential of the $Ru^{2+/3+}$ redox pair changes by 1.0 eV when going from the aqueous hexaaquo-complex to the aqueous bipyridine complex ($\varepsilon^0 = 0.23$ eV[1] for $Ru(H_2O)_6^{2+/3+}$ and 1.24 eV[1] for $Ru(bpy)_3^{2+/3+}$, bpy = 2,2′-bipyridine). What is the origin of this difference? A quantum chemists' approach to this question would be to describe oxidation by a thermodynamic cycle and explain the difference in redox potential by the difference in ionization potential of the solute in the gas phase and the differences in hydration free energy of the reduced and oxidized ion. Our approach takes an alternative route that is closer to the view of an electrochemist, see Figure 1. Remaining entirely in the condensed phase, we describe oxidation reactions as a sum of two events, (i) ionization of the solvated ion at fixed nuclear configuration but with relaxed $N - 1$ electrons and (ii) relaxation or reorganization of the nuclei from the equilibrium structure of the reduced state to the equilibrium structure of the oxidized state. The absolute oxidation free enthalpy, ΔG^0, is then composed of two contributions, the vertical ionization energy, denoted ΔE_R in Figure 1, and the reorganization free energy of the oxidized state, denoted λ_O.

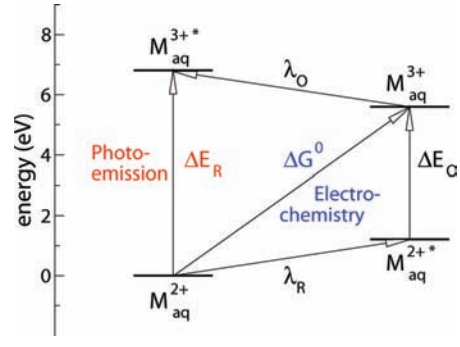

Figure 1. Redox properties accessed by photoemission spectroscopy and electrochemistry. ΔE_R is the vertical ionization energy (or electron binding energy E_b of the HOMO) of the reduced state M^{2+}_{aq}, ΔE_O is the vertical electron affinity of the oxidized state M^{3+}_{aq}, ΔG^0 is the standard free enthalpy difference of oxidation (or adiabatic ionization free enthalpy) corresponding to the absolute redox potential, and λ_O is the reorganization free energy relating the free energy of the vertical state M^{3+*}_{aq}, to the relaxed equilibrium state of the same oxidation state, M^{3+}_{aq}, and similarly for λ_R. See section 2 for a statistical mechanics definition of these quantities.

[†] Helmholtz-Zentrum Berlin für Materialien und Energie, and BESSY.
[‡] Max-Planck-Institut für Dynamik and Selbstorganisation.
[§] University of Cambridge.

(1) Lide, D. R., Ed. *CRC Handbook of Chemistry and Physics*, 75th ed.; CRC Press: Boca Raton, FL, 1995.

The reorganization free energy plays an important role not only for thermochemistry but, according to Marcus theory, also for the kinetics of redox reactions by determining the activation free energy for oxidation or electron transfer (together with redox potential).

The question we investigate in this work is whether the large difference in redox potential between aqueous $Ru(bpy)_3^{2+/3+}$ and $Ru(H_2O)_6^{2+/3+}$ is associated with the difference in vertical ionization energy or with the difference in reorganization free energy of the two ions. There are two experimental methods that should help us quantify these two different contributions: photoemission spectroscopy (PES), which yields the vertical binding or photodetachment energy of the highest occupied molecular orbital (HOMO), denoted E_b, and electrochemistry, which yields adiabatic oxidation free enthalpy, ΔG^0. The photo effect process typically occurs on the subfemtosecond time scale, which is too fast for nuclear relaxation to occur.[2,3] Thus, E_b can be identified with ΔE_R and the difference between E_b and ΔG^0 with the reorganization free energy of the oxidized ion,

$$\lambda_O^b = E_b - \Delta G^0 + e\Delta\kappa \quad (1)$$

where we have added a term $e\Delta\kappa$ accounting for the (small) potential difference between solution and vapor phase; e is the unit charge.

Estimation of reorganization free energies from PE spectra has been pioneered by Delahay and co-workers[4−7] and further continued by Watanabe and co-workers.[8] Using tunable vacuum UV light up to 10 eV, the ionization threshold energy of a large number of aqueous solutions of inorganic anions and cations could be determined for the first time. The reorganization free energy was estimated according to eq 1 by using the threshold energy E_t instead of the binding energy E_b of the HOMO. The former was determined from a linear extrapolation of the square-root of the yield, which corresponds to an energy at the tail of the peak of the HOMO level. The latter is the energy at the center of the peak which could not be measured in these early experiments. Yet, the difference between E_t and E_b can be substantial: $E_t = 9.9$ eV for liquid water, whereas the center of the $1b_1$ peak (HOMO) is at $E_b = 11.16$ eV[2] (note that the binding energy is defined positive here as opposed to previous work[2]). Thus, using E_t as an approximation to the vertical ionization energy, E_b and λ_O^b can be underestimated by 1 eV or more.

With the development of a novel liquid microjet technique, it has become possible to measure energy-resolved photoemission spectra and thus E_b values of aqueous solutions quite accurately.[2,9] This method has been applied to the measurement of PE spectra of water and alcohols,[2,9] aqueous solutions of halide ions,[2,9,10] hydronium and hydroxide ions,[11] and imidazole.[3,12] However, no measurements have been reported for redox-active aqueous transition metal ions. Here we report the first PE spectrum of this kind for $Ru(bpy)_3^{2+}$ in aqueous solution. From the PE spectrum we obtain the binding energy of the HOMO, E_b, and since the redox potential is well-known, we report the experimental reorganization free energy λ_O^b of $Ru(bpy)_3^{3+}$ by virtue of eq 1.

Energy resolved PES provides a unique opportunity for investigating the reliability of computational methods in estimating reorganization free energy. In previous work Blumberger, Sprik and co-workers have reported reorganization free energies for aqueous transition metal ions, $Ag^{+/2+}$,[13,14] $Cu^{+/2+}$,[13,15] $Ru^{2+/3+}$,[16,17] and $RuO_4^{2-/-}$,[18,19] using density functional molecular dynamics simulation. The simulated systems typically comprised of one ion solvated by about 30 water molecules. The classical ion dynamics is propagated on the Born−Oppenheimer surface and the redox potential, ionization potential and reorganization free energy obtained from the vertical energy gap in the reduced and oxidized states (see section 2). In the present work we apply this approach to aqueous $Ru(bpy)_3^{2+/3+}$ and compare with the experimental results obtained from PES. After validation against experiment, which requires a correction for the finite simulation cell used, we carry out similar calculations for aqueous $Ru(H_2O)_6^{2+/3+}$. The difference to previous simulations[16,17] of this redox pair is that we can now afford to treat a significantly larger solvation shell of more than 100 water molecules allowing us to characterize the full second solvation shell. PES data are not available for the hexaaquo-ions because $Ru(H_2O)_6^{2+}$ is unstable against oxidation under experimental conditions.

We find that experimental and computed reorganization free energy agree fairly well even though the computed numbers are sensitive to the method used to extrapolate to the infinite dilution limit. According to our calculations the large difference in redox potential between $Ru(bpy)_3^{2+/3+}$ and $Ru(H_2O)_6^{2+/3+}$ is associated with the different reorganization free energies of the oxidized ions, rather than the difference in the vertical ionization potential of the reduced ion. The difference in reorganization free energy is about 1 eV (≈ redox potential difference) and originates from the very different nuclear response of these ions to oxidation. While the Ru−N bonds in $Ru(bpy)_3^{2+}$ hardly change upon oxidation there is a significant change in the Ru−O bond lengths upon oxidation of $Ru(H_2O)_6^{2+}$ ("inner sphere" reorganization). However most of the difference is related to the response of the second and higher solvation shells ("outer sphere" reorganization free energy). $Ru(bpy)_3^{2+}$ forms a large hydrophobic cavity in aqueous solution which leads to a much smaller dipolar response of second and higher solvation shells than in the case of the hydrophilic $Ru(H_2O)_6^{2+}$ ion.

This paper is organized as follows. In the next section we review the statistical mechanics of redox reactions which provides the theoretical framework for calculation of redox properties from molecular dynamics simulation. In section 3

(2) Winter, B.; Faubel, M. *Chem. Rev.* **2006**, *106*, 1176.
(3) Jagoda-Cwiklik, B.; Slavicek, P.; Cwiklik, L.; Nolting, D.; Winter, B.; Jungwirth, P. *J. Phys. Chem. A* **2008**, *112*, 3499.
(4) Delahay, P.; von Burg, K.; Dziedzic, A. *Chem. Phys. Lett.* **1981**, *79*, 157.
(5) Delahay, P. *Chem. Phys. Lett.* **1982**, *90*, 425.
(6) Delahay, P. *Acc. Chem. Res.* **1982**, *15*, 40.
(7) Delahay, P.; Dziedzic, A. *J. Chem. Phys.* **1984**, *80*, 5793.
(8) Watanabe, I.; Ono, K.; Ikeda, S. *Bull. Chem. Soc. Jpn.* **1991**, *64*, 352.
(9) Faubel, M. In *Photoionization and photodetachment*; Ng, C. Y., Ed.; World Scientific: Singapore, 2000; Vol. 10A, Part 1, p 634.
(10) Winter, B.; Weber, R.; Hertel, I.; Faubel, M.; Jungwirth, P.; Brown, E.; Bradforth, S. *J. Am. Chem. Soc.* **2005**, *127*, 7203.
(11) Winter, B.; Faubel, M.; Hertel, I.; Pettenkofer, C.; Bradforth, S.; Jagoda-Cwiklik, B.; Cwiklik, L.; Jungwirth, P. *J. Am. Chem. Soc.* **2006**, *128*, 3864.
(12) Jagoda-Cwiklik, B.; Slavicek, P.; Nolting, D.; Winter, B.; Jungwirth, P. *J. Phys. Chem. B* **2008**, *112*, 7355.
(13) Blumberger, J.; Bernasconi, L.; Tavernelli, I.; Vuilleumier, R.; Sprik, M. *J. Am. Chem. Soc.* **2004**, *126*, 3928.
(14) Blumberger, J.; Tavernelli, I.; Klein, M. L.; Sprik, M. *J. Chem. Phys.* **2006**, *124*, 64507.
(15) Blumberger, J. *J. Am. Chem. Soc.* **2008**, *130*, 16065.
(16) Blumberger, J.; Sprik, M. *J. Phys. Chem. B* **2005**, *109*, 6793.
(17) Blumberger, J.; Sprik, M. *Theor. Chem. Acc.* **2006**, *115*, 113.
(18) Tateyama, Y.; Blumberger, J.; Sprik, M.; Tavernelli, I. *J. Chem. Phys.* **2005**, *122*, 234505.
(19) Tateyama, Y.; Blumberger, J.; Ohno, T.; Sprik, M. *J. Chem. Phys.* **2007**, *126*, 204506.

details of the experimental measurement of PE spectrum and of the computations are specified. The PE spectrum of $Ru(bpy)_3^{2+}$ is presented and discussed in the first part of section 4. In the second part the results of density functional molecular dynamics (DFMD) simulation of $Ru(bpy)_3^{2+}$, $Ru(bpy)_3^{3+}$, $Ru(H_2O)_6^{2+}$ and $Ru(H_2O)_6^{3+}$ are reported including solvation structure, redox potential and reorganization free energy. At the end of section 4 we compare the PE spectrum of aqueous $Ru(bpy)_3^{2+}$ with the Kohn−Sham density of states and interpret occupied and virtual energy levels of the solute. The work is concluded in section 5.

2. Theoretical Background

The classical statistical mechanics of oxidation reactions

$$\mathrm{R} \rightarrow \mathrm{O} + 1e^- \tag{2}$$

has been recently reviewed by one of us.[20] Here we briefly summarize the formulas used in the calculations presented in section 4. In eq 2 R and O denote the total system containing solute and solvent in the reduced and oxidized state, respectively. The basic quantity in our approach for calculation of free energies for reaction eq 2 is the vertical, electronically relaxed ionization energy at fixed ionic configuration $\mathbf{R}^N$ (energy gap)

$$\Delta E(\mathbf{R}^N) = E_\mathrm{O}(\mathbf{R}^N) - E_\mathrm{R}(\mathbf{R}^N) \tag{3}$$

where $E_M(\mathbf{R}^N)$, M = R, O, is the ground state potential energy surface of reactant and product, respectively. When computed along a trajectory of state R the gap energy is denoted ionization energy, and when computed along a trajectory of state O it is denoted electron affinity. It turns out that the energy gap is a good reaction coordinate for solvent controlled oxidation reactions. Hence, in Marcus theory of oxidation[21] the probability distributions of the thermal fluctuations of the energy gap, p_M, are taken to construct diabatic free energy curves of initial (M = R) and final (M = O) state, A_M:[22]

$$A_M(\Delta E') = -k_\mathrm{B}T \ln p_M(\Delta E') + \mathrm{const} \tag{4}$$

$$p_M = \langle \delta(\Delta E(\mathbf{R}^N) - \Delta E') \rangle_M \tag{5}$$

where δ is the Dirac delta function, k_B is the Boltzmann constant, and T is the temperature. Brackets $\langle \cdots \rangle_M$ denote the usual canonical average in state M. The diabatic curves define the reorganization free energy as the cost in free energy when distorting the ions from the equilibrium position of one diabatic state to the equilibrium position of the other state while remaining on the same diabatic free energy curve (see also Figure 1),

$$\lambda_\mathrm{R} = A_\mathrm{R}(\Delta E_\mathrm{O}^{\min}) - A_\mathrm{R}(\Delta E_\mathrm{R}^{\min}) \tag{6}$$

$$\lambda_\mathrm{O} = A_\mathrm{O}(\Delta E_\mathrm{R}^{\min}) - A_\mathrm{O}(\Delta E_\mathrm{O}^{\min}) \tag{7}$$

where $\Delta E_M^{\min}$ is the position of the minimum of the diabatic free energy curve of M. Inserting the linear free energy relation $A_\mathrm{O} - A_\mathrm{R} = \Delta E$ (ref 23) in eq 7, one obtains

$$\lambda_\mathrm{O} = \Delta E_\mathrm{R}^{\min} - \Delta A' \tag{8}$$

where $\Delta A'$ is the driving force of reaction eq 2, $\Delta A' = A_\mathrm{O}(\Delta E_\mathrm{O}^{\min}) - A_\mathrm{R}(\Delta E_\mathrm{R}^{\min})$. Note that $\Delta A'$ equals exactly the oxidation free energy ΔA in the limit of linear response[20] but $\Delta A' \approx \Delta A$ is usually a good approximation for systems that are not in the linear response regime.[14,15] Equation 8 provides the theoretical basis for obtaining reorganization free energies of the oxidized ion from PE spectra. Identifying $\Delta E_\mathrm{R}^{\min}$ with the binding energy E_b of the electron in the highest occupied orbital (HOMO) and $\Delta A'$ with the absolute oxidation free enthalpy ΔG^0 one obtains eq 1. Note that the difference between enthalpies and energies is very small in condensed phase systems and is thus neglected.

Computationally, the diabatic free energy curves and reorganization free energies can be obtained from DFMD combined with umbrella sampling.[14,15,22] The amount of computation can be drastically reduced, however, if the system is in the linear response limit. This is the case if the fluctuations of ΔE are Gaussian in either of the two states R or O. Then the following identities hold.[18]

$$\lambda = \lambda_\mathrm{R} = \lambda_\mathrm{O} = (\Delta E_\mathrm{R} - \Delta E_\mathrm{O})/2 \tag{9}$$

$$\lambda = \sigma^2/(2k_\mathrm{B}T) \tag{10}$$

$$\sigma = \sigma_\mathrm{R} = \sigma_\mathrm{O} \tag{11}$$

$$\Delta A = \Delta A' = (\Delta E_\mathrm{R} + \Delta E_\mathrm{O})/2 \tag{12}$$

where

$$\Delta E_M = \langle \Delta E \rangle_M \tag{13}$$

In eqs 11 and 12 σ_M is the width of energy gap fluctuations in state M and ΔA is the oxidation free energy of reaction eq 2. Thus, in the linear response regime λ and ΔA can be conveniently calculated from the average energy gaps eq 3 sampled along molecular dynamics trajectories in state R and O, respectively. In the Supporting Information (SI) of this article, we describe two more approximate methods for calculation of redox properties, one based on a combination of gas phase density functional calculation and classical molecular dynamics simulation (QM+MM) and one where the solvent is treated as a continuum.

3. Methods

3.1. Photoemission Spectroscopy. PES measurements for 0.2 m $Ru(bpy)_3^{2+}$ [Tris(2,2′-bipyridine) dichlororuthenium(II) hexahydrate] aqueous solution were performed at the U41 PGM undulator beamline of the synchrotron radiation facility BESSY, Berlin. PE spectra were collected from a 15-μm vacuum liquid microjet traveling at a velocity of 120 ms^{-1} with a temperature of 4 °C. In the present valence photoelectron study we have used a photon energy of 200 eV. Details of the technique and of the experimental setup have been described previously.[2] Briefly, electrons were detected normal to both the synchrotron light polarization vector and the flow of the liquid jet. Photoelectrons pass through a 200 μm diameter orifice, which separates the main interaction chamber (operating at 10^{-5} mbar) from the differentially pumped detector chamber (operating at 10^{-9} mbar) housing a hemispherical electron energy-analyzer, equipped with a multichannel detector. The orifice is at a distance of 1.0 mm from the liquid jet. Energy resolution of the U41 beamline was better than 200 meV at the incident photon energy used here, and the resolution of the hemispherical energy analyzer was constant with kinetic energy (about 200 meV, at 20

(20) Blumberger, J. *Phys. Chem. Chem. Phys.* **2008**, *10*, 5651.
(21) Marcus, R. A. *J. Chem. Phys.* **1965**, *43*, 679.
(22) Warshel, A. *J. Phys. Chem.* **1982**, *86*, 2218.
(23) Tachiya, M. *J. Phys. Chem.* **1989**, *93*, 7050.

eV pass energy). Typical count rates were 10^3-10^4 s^{-1}. The small focal size (23×12 μm^2) of the incident photon beam allows for matching spatial overlap with the liquid microjet, and limits the contribution of gas-phase components in the collected PE spectra to <5% for liquid water. Measured electron kinetic energies are given with reference to the $1b_1$ binding energy of liquid water.[2] Highly demineralized water was used for preparing the 0.2 m $Ru(bpy)_3^{2+}$ aqueous solution; the salt was of the highest quality commercially available (>99.5%, Sigma-Aldrich).

3.2. Simulation Details. Gas-Phase Calculations. The geometries and potential energies of gas-phase $Ru(bpy)_3^{2+}$ and $Ru(bpy)_3^{3+}$ were optimized at the PBE[24]/LANL2DZ, BLYP[25,26]/LANL2DZ and B3LYP[27]/LANL2DZ level of theory using the Gaussian program and applying default convergence criteria.[28] For $Ru(H_2O)_6^{2+}$ and $Ru(H_2O)_6^{3+}$ calculations were carried out at the BLYP/LANL2DZ level of theory. The oxidized states (+3) were treated as doublets, the reduced states (+2) as singlets. The potential energies of the PBE/LANL2DZ structures of $Ru(bpy)_3^{2+}$ and $Ru(bpy)_3^{3+}$ were also calculated at the PBE/TZV2P level of theory using the mixed localized/plane wave basis set program CP2K.[29] Here and in the following the TZV2P (DZVP) basis denotes the TZV2P (DZVP) basis set for valence electrons of H,C,N,O and the TZV (TZV) basis for Ru. Goedecker−Teter−Hutter (GTH[30]) pseudopotentials are used to represent the core of H,C,N,O. A 16-electron semicore GTH pseudopotential is used for Ru. The reciprocal space density cutoff for the auxiliary plane wave basis is 280 Ry.

Classical Molecular Dynamics Simulations. Classical molecular dynamics simulations were carried out using the Amber 9 program package.[31] Aqueous solutions of $Ru(bpy)_3^{2+}$ and $Ru(bpy)_3^{3+}$ were prepared containing one solute molecule and 104, 206, 345, 519, 1160, 2555, 5456, and 10057 POL3 water[32] molecules per unit cell. Solutions of $Ru(H_2O)_6^{2+}$ and $Ru(H_2O)_6^{3+}$ contained one Ru ion and 65, 128, 259, 515, 1022, 2046, and 5699 POL3 water molecules per unit cell. The force field parameter for $Ru(bpy)_3^{2+}$ and $Ru(bpy)_3^{3+}$ and the RESP charges of the bpy ligands were taken from a previous study of the $Ru(bpy)_3^{2+}$ (im)(his) chromophore.[20] A total charge of +2 and +3 was enforced by adding the remaining charge to the Ru atom. The force field parameter and point charges for $Ru(H_2O)_6^{2+}$ and $Ru(H_2O)_6^{3+}$ were taken from a recent electron self-exchange study of the two ions.[33] The point charges used for all four complexes are summarized in Table 4 in the SI. All solute atoms (including the first solvation shell of the aquo-complexes) were treated nonpolarizable. The induced dipoles of the POL3 water molecules were calculated self-consistently at each molecular dynamics time step using the default convergence criterion. The electrostatic energy was calculated using Ewald summation, Lennard-Jones interactions were truncated at 10 Å or at a distance half the box length if the latter was smaller than 20 Å. The solutions were equilibrated in a cubic unit cell at a target temperature of 300 K and pressure of 1 bar for 200 ps and equilibrated for a further 200 ps in the NVT ensemble. The next 1 ns of dynamics was used for calculation of the total electrostatic energy gap in periodic boundary conditions (eq 7 in the SI). The energy gap includes both the contribution of the permanent point charges and of the induced dipoles.

(24) Perdew, J. P.; Burke, K.; Ernzerhof, M. *Phys. Rev. Lett.* **1996**, *77*, 3865.
(25) Becke, A. D. *Phys. Rev. A* **1988**, *38*, 3098.
(26) Lee, C.; Yang, W.; Parr, R. *Phys. Rev. B* **1988**, *37*, 785.
(27) Becke, A. *J. Chem. Phys.* **1993**, *98*, 5648.
(28) Frisch, M. J.; et al. *Gaussian 03, Revision C.01*; Gaussian, Inc.: Wallingford, CT, 2004.
(29) Quickstep, CP2K Developers Group, http://www.cp2k.berlios.de.
(30) Goedecker, S.; Teter, M.; Hutter, J. *Phys. Rev. B* **1996**, *54*, 1703.
(31) Case, D. A.; et al. *AMBER 9*; University of California: San Francisco, 2006.
(32) Caldwell, J. W.; Kollman, P. A. *J. Phys. Chem.* **1995**, *99*, 6208.
(33) Blumberger, J.; Lamoureux, G. *Mol. Phys.* **2008**, *106*, 1597.

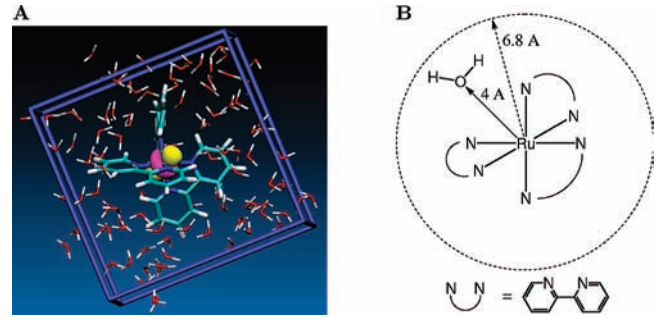

Figure 2. (A) Snapshot of aqueous $Ru(bpy)_3^{2+}$ taken from a density functional molecular dynamics trajectory. Only one unit cell of the periodically replicated system is depicted (purple lines) containing one solute molecule (drawn as thick sticks, center) and 104 water molecules (drawn as thin sticks). Color code: H: white, C: dark green, N: blue, O: red, Ru: light green. Isosurfaces of the highest occupied orbital (HOMO) of aqueous $Ru(bpy)_3^{2+}$ are depicted in yellow and pink, respectively. (B) Solute molecule $Ru(bpy)_3^{2+}$ in a 2-dimensional representation. The closest approach of a water molecule along a 10 ps MD trajectory is indicated. The cavity formed by the hydrophobic bpy ligands is depicted in dashed lines. The cavity radius is equal to the average Ru−H(@bpy) distance of 6.0 Å, plus the atomic radius of a hydrogen atom, 0.8 Å.

Density Functional Molecular Dynamics Simulations. A classical configuration of the 104 water molecule system of $Ru(bpy)_3^{2+}$ was taken as initial configuration for the DFMD run, see Figure 2. The system was equilibrated at 330 K in the NVT ensemble for 4.7 ps at the PBE/TZV2P level of theory, which was followed by 5.5 ps production run. Then the system was equilibrated for 4.5 ps at the PBE/DZVP level of theory followed by 5 ps production run. The energy gap eq 3 was calculated at the PBE/TZV2P level of theory for 550 equidistantly spaced snapshots taken from the PBE/TZV2P trajectory and for 494 equidistantly spaced snapshots taken from the PBE/DZVP trajectory. The average was 1.85 eV for the former and 1.88 eV for the latter indicating that for our purposes the DZVP basis set is sufficiently large for generation of molecular dynamics trajectories. The gap energies calculated for both trajectories was taken for further analysis. Similarly, a classical configuration of the 104 water molecule system of $Ru(bpy)_3^{3+}$ was taken as initial configuration for the density functional molecular dynamics simulation of the oxidized state. The system was equilibrated at 330 K for 5 ps followed by 9.7 ps production run at the PBE/DZVP level of theory. The energy gap eq 3 was calculated for 488 snapshots at the PBE/TZV2P level of theory. The density functional simulations for $Ru(H_2O)_6^{2+}$ and $Ru(H_2O)_6^{3+}$ were carried out similarly. The molecular dynamics and energy gap calculations of all four aqueous solutions were carried out for a cubic periodic box of length 15.84 Å. In the dynamics runs a time step of 0.5 fs was used and a chain of Nose-Hoover thermostat was used with the default coupling parameter. Pseudopotentials and electronic structure method are the same as described above. A wave function convergence criterion of at least 5×10^{-6} H was applied ensuring a drift of the conserved energy of less than 1×10^{-4} a.u. atom $^{-1}$ ps $^{-1}$. Kohn−Sham orbital energies of aqueous $Ru(bpy)_3^{2+}$ were calculated at the PBE/TZV2P level of theory for 99 equidistantly spaced snapshots taken from the PBE/DZVP trajectory.

4. Results and Discussion

4.1. PE Spectrum of Aqueous $Ru(bpy)_3^{2+}$. The valence PE spectrum of 0.2 m $Ru(bpy)_3^{2+}$ aqueous solution, measured at 200 eV photon energy, is presented in Figure 3. This spectrum is almost identical with the one of pure water, except for the low electron binding energy (BE) region, at approximately 6−10 eV BE. The peak position of the four valence bands of liquid water, $1b_1$, $3a_1$, $1b_2$, and $2a_1$, are virtually identical with the

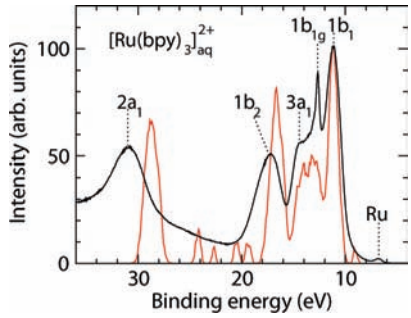

Figure 3. Photoemission spectrum of aqueous $Ru(bpy)_3^{2+}$ (black line) and computed density of states (red line). See section 3 for experimental details. The computed binding energies are equal to minus the Kohn−Sham orbital energies. The latter were calculated for 99 snapshots taken from a density functional molecular dynamics simulation of length 5 ps, and collected in bins of width 0.1 eV. The center and height of the $1b_1$ peak of the computed density of states is aligned with the corresponding experimental peak. Calculations were carried out at the PBE/TZV2P level of theory.

values reported in ref 34. BEs were determined as the energy shift from the $1b_1$ $H_2O(aq)$ BE which is 11.16 eV[34] with respect to vacuum. The spectral region with the small solute emission intensity at BEs lower than for the water $1b_1$ peak is shown magnified (curve 1) in Figure 4a, where we also present the PE spectrum of pure water (curve 2) for comparison. Subtraction of the two spectra, (1)−(2), after intensity normalization at background signal near 40 eV BE, and at $1b_1$ signal (see Figure 3), yields the differential spectrum (circles) shown in Figure 4b. It exhibits two distinct peaks, at 9.60 and 6.81 eV BE, and there is some additional solute contribution at approximately 8.20 eV BE.

The peak at 6.81 eV (uncertainty = 0.04 eV, full width at half-maximum (fwhm) = 0.7 eV) is due to photoemission from the HOMO level of $Ru(bpy)_3^{2+}$. The peak at 9.60 eV is predominantly due to Cl^- 3*p*(aq) photoemission from the chloride counterion. To qualitatively account for this latter contribution we also show in Figure 4b the Cl^- 3*p*(aq) PE peak (curve 3) obtained from a 2 m NaCl aqueous solution. As above it is also the difference spectrum, that is, solution minus water spectral intensity, represented by a Gaussian fit. Peak position and width (fwhm = 0.7 eV) are the same as previously reported for alkali-chloride aqueous solutions.[2] The Cl^- peak height (curve 3) was evaluated from comparison of the PE signal intensity ratios $1b_1/Cl^-$ 3p and $1b_1$/Ru HOMO. When accounting for the five times higher chloride concentration in the NaCl solution as compared to the 0.2 m dichloro-$Ru(bpy)_3^{2+}$ solution the chloride signal is calculated to be × 2.1 larger than for the HOMO of $Ru(bpy)_3^{2+}$. In Figure 4b, the peak height of (3) is hence set to correspond to 2.1 larger peak area than for the HOMO of $Ru(bpy)_3^{2+}$. The very good match of curve (3) and the difference spectrum (1)−(2) in the 9 to 10 eV BE region implies that intensity is entirely from Cl^-3*p*(aq) emission. The detailed spectral assignment relies on electronic structure calculations which are discussed in section 4.2.5.

The reorganization free energy of aqueous $Ru(bpy)_3^{3+}$ is determined from the PE spectrum according to eq 1. The absolute binding energy of the HOMO level of $Ru(bpy)_3^{2+}$ is E_b = 6.81 eV and the absolute oxidation free enthalpy is ΔG^0 = 5.60 eV using the tabulated reduction potential for aqueous $Ru(bpy)_3^{3+/2+}$ versus normal hydrogen electrode (NHE), 1.24 V,[1]

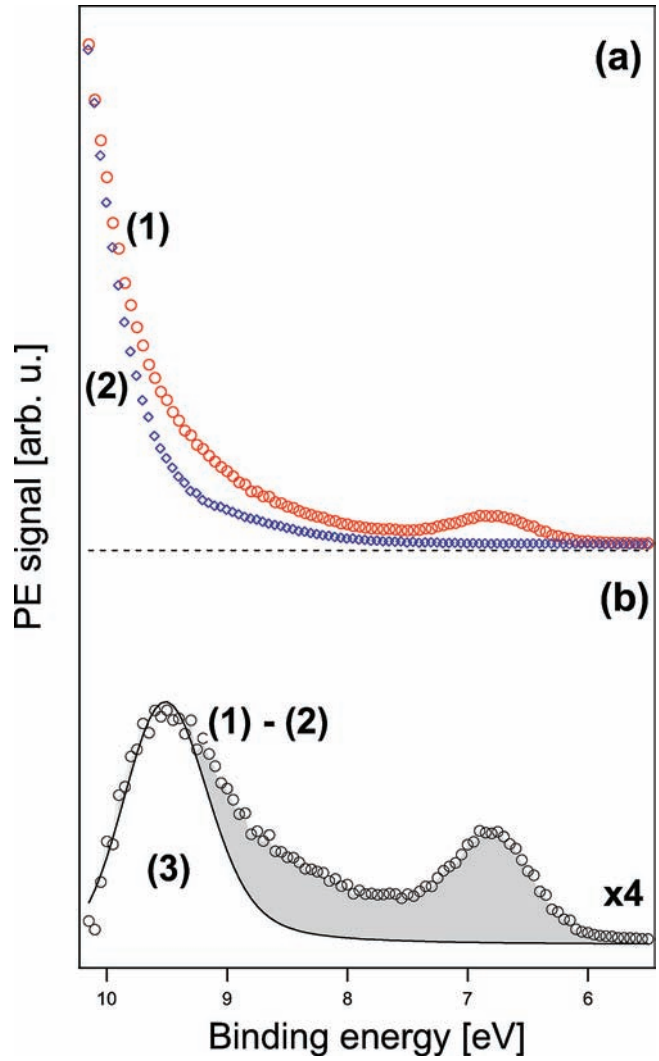

Figure 4. (a) Enlarged view of the onset of photoemission from 0.2 m aqueous $Ru(bpy)_3^{2+}$ (curve (1), red circles). The PE spectrum of pure water is shown for comparison (curve (2), blue circles). (b) Dfferential spectrum, (1)−(2), is contrasted with the PE spectrum of a 2 m NaCl aqueous solutions (solid line), to illustrate the spectral contributions arising from Cl^-_{aq} photoemission. The gray-shaded area highlights the intensity due to the metal complex. See Figure 3 for the full valence spectrum.

and a value of 4.36 V for the absolute half cell potential of the NHE.[35] The latter was obtained using a formation free enthalpy of 1517.1 ± 0.3 kJ/mol for the $1/2\ H_{2,g} \rightarrow H_g^+ + e_g^-$ reaction, a solvation free enthalpy of −1104.5 kJ/mol for the H_g^+ ion (Tissandier et al.[36]), and a work term of 7.9 kJ/mol to convert between the standard concentrations of the proton in the gas and solution phase.[35] We note that the solvation free enthalpy of H_g^+ is interpreted as arising from solvation only; it does not include the work against the surface potential required for the transfer of the proton from the vapor to the liquid phase. In present PE experiments the surface potential term in eq 1 is expected to be negligibly small ($e\Delta\kappa$ < 10 meV for pure water jets[2]). The binding energy obtained from PES can then be directly compared with the absolute half cell potential determined as discussed above. The result is an experimental estimate

(34) Winter, B.; Weber, R.; Widdra, W.; Dittmar, M.; Faubel, M.; Hertel, I. V. *J. Phys. Chem. A* **2004**, *108*, 2625.

(35) Lewis, A.; Bumpus, J. A.; Truhlar, D. G.; Cramer, C. J. *J. Chem. Educ.* **2004**, *81*, 596.

(36) Tissandier, M. D.; Cowen, K. A.; Feng, W. Y.; Gundlach, E.; Cohen, M. H.; Earhart, A. D.; Coe, J. V.; Tuttle, T. R. *J. Phys. Chem. A* **1998**, *102*, 7787.

Table 1. Computed Structural Properties of $Ru(bpy)_3^{2+}$, $Ru(bpy)_3^{3+}$, $Ru(H_2O)_6^{2+}$ and $Ru(H_2O)_6^{3+}$ in the Gas Phase at 0 K (g) and in Aqueous Solution (aq) at 300 K from Density Functional Molecular Dynamics Simulation[a]

	$Ru(bpy)_3^{2+}$	$Ru(bpy)_3^{3+}$
Ru−N (g) (Å)	2.07[b] (2.053[c])	2.09[b] (2.057[c])
Ru−N (aq) (Å)	2.08[d]	
	2.08[e]	2.10[e]
CN(RuO)	7[d,f]	
	5[e,f]	9[e,f]
Ru−O (g) (Å)	2.16[g] (2.122[h])	2.10[g] (2.029[h])
g(RuO) (aq)		
1. max (Å)	2.16[d] (2.11[i])	2.08[e] (2.03[i])
CN(1.shell)	6	6
2. max (Å)	3.8−4.3	4.18
CN(2.shell)	18[j]	18[j]

[a] Experimental values are given in parentheses. g(RuO) denotes the radial distribution function between Ru and O atoms and CN denotes the coordination number obtained by spherical integration of the radial distribution function. [b] PBE[24]/LANL2DZ. [c] Reference 38; bond lengths in crystals. [d] PBE/TZV2P. [e] PBE/DZVP. [f] g(RuO) integrated up to a distance of 6.08 Å. [g] BLYP[25,26]/LANL2DZ. [h] Reference 39. [i] Reference 53. [j] g(RuO) integrated up to a distance of 4.96 Å(Ru^{2+}) and 4.74 Å(Ru^{3+}).

for reorganization free energy of $\lambda_O^b = E_b - \Delta G^0 = 1.21 \pm 0.04$ eV, which will be compared to our computed estimate in section 4.2.3. Note that the binding energy used for calculation of λ_O^b is for a solution 0.2 m in $Ru(bpy)_3^{2+}$. Based on previous PE studies of various aqueous solutions, we expect the effect of concentration on the measured binding energy to be very small. For instance, the shift of the binding energy of aqueous iodide ions (I^- 5p and I^- 4d) was less than 30 meV when going from 0.1 m NaI to 12 m NaI concentration.[37] This suggests that the reorganization free energy reported herein is a good approximation to the hypothetical limit of infinite dilution.

4.2. Calculations. 4.2.1. Solvation Structure. The coordination geometry and solvation structures obtained from DFMD of the Ru-complexes are summarized in Table 1. The $Ru(bpy)_3^{2+}$ complex forms a regular octahedron with Ru−N distances that are rather insensitive to oxidation state and finite temperature fluctuations of the environment. Oxidation to $Ru(bpy)_3^{3+}$ leads to an increase of the Ru−N distances by 0.02 Å in the gas phase and in aqueous solution. The combined effect of solvation and finite temperature is a small increase of the Ru−N distances by 0.01 Å in both oxidation states. The small deviation between the computed bond length for $Ru(bpy)_3^{2+}$, 2.07 Å, and the crystal structure, 2.053 Å,[38] indicates that the PBE functional describes the structure of $Ru(bpy)_3^{2+}$ fairly well. BLYP and B3LYP perform slighty worse, with bond lenghts predicted to be 2.11 and 2.10 Å, respectively.

The apolar hydrogen atoms of the bpy ligands create a hydrophobic environment around the Ru^{2+} ion preventing solvent molecules from penetrating the void between the ligands, see Figure 2. The closest approach of a solvent molecule occurs at an angle of about 45 degrees, symmetrically intersecting the angle N−Ru−N at a distance of about 4 Å, measured between the Ru ion and the oxygen atom of solvent molecules. The Ru−O and Ru−H radial distribution functions of $Ru(bpy)_3^{2+}$ do not exhibit any major structural features, see Figure 5. The

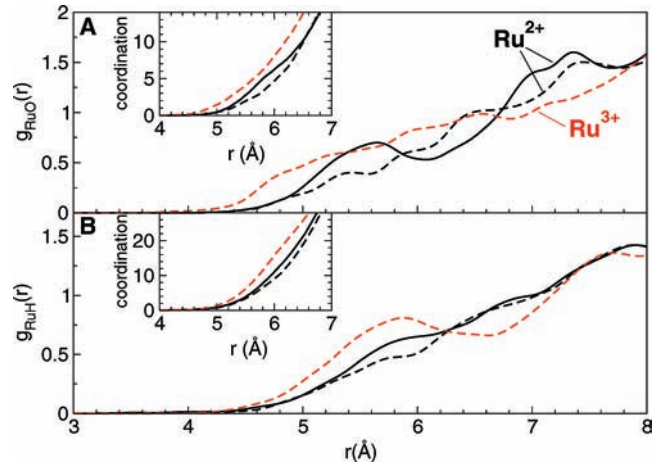

Figure 5. Radial distribution function $g(r)$ between the Ru atom of the solute, $Ru(bpy)_3^{2+}$, and the O-atoms (A) and H-atoms (B) of water molecules (black). The corresponding radial distribution functions for $Ru(bpy)_3^{3+}$ are shown in red. The coordination numbers obtained by spherical integration of the radial distributions are shown in the insets. A unit cell contains one solute molecule and 104 water molecules; (—) PBE/TZV2P, (- - -) PBE/DZVP. Data points were collected in bins of width 0.01 Å and the distributions were smoothed by convolution with a Gaussian of width 0.03 Å.

onset of both distributions is at similar distances indicating that there is no specific radial alignment of the dipole moment of the closest water molecules. The details of the distributions are somewhat sensitive to the basis set used. At the PBE/DZVP level of theory the radial distributions are featureless, whereas at the PBE/TZV2P level a small and broad peak appears at 5−6 Å. The Ru−O coordination number, calculated by integrating the radial distribution function in spherical shells up to 6.08 Å, is 7 and 5 water molecules at the PBE/TZV2P and PBE/DZVP level of theory, respectively. Oxidation to $Ru(bpy)_3^{3+}$ leads to an increase in coordination number from 5 to 9 (at 6.08 Å) at the PBE/DZVP level of theory, but it does not induce a greater penetration of the empty space between the ligands.

The solvation structures obtained for the octahedral ions $Ru(H_2O)_6^{2+}$ and $Ru(H_2O)_6^{3+}$ are very similar to the ones reported previously.[17,16] Present simulations were carried out for a Ru-ion solvated by 128 water molecules using the PBE functional and a localized basis set (TZV2P for $Ru(H_2O)_6^{2+}$ and DZVP for $Ru(H_2O)_6^{3+}$). Previous simulations were carried out for solutions containing 32 water molecules using the BLYP functional and a plane wave basis set. Despite these differences only minor deviations in the radial distribution functions are found, with the position of the first peak coinciding to 0.01 Å with the previously reported value, see Figure 6. This indicates that the first shell solvation structure is little dependent on the number of water molecules used, even though this could be partly due to some cancellation effects caused by the different basis sets and density functional used. In contrast to $Ru(bpy)_3^{2+}$ we observe a significant change in metal−oxygen bond lengths upon oxidation of $Ru(H_2O)_6^{2+}$. The Ru−O bonds decrease by 0.08 Å, in excellent agreement with experiment[39] and previous simulations.[16,17]

The larger system size used in this study permits also the characterization of the second solvation shell. While the Ru−O radial distribution of $Ru(H_2O)_6^{3+}$ exhibits a clear second peak at 4.18 Å, the peak for $Ru(H_2O)_6^{2+}$ is broad and we can only give a rough estimate for its position, 3.8−4.3 Å. The radial distribution integrated up to the second minimum is 18 in both

(37) Weber, R.; Winter, B.; Schmidt, P. M.; Widdra, W.; Hertel, I. V.; Dittmar, M.; Faubel, M. *J. Phys. Chem. B* **2004**, *108*, 4729.
(38) Biner, M.; Büergi, H.-B.; Ludi, A.; Röhr, C. *J. Am. Chem. Soc.* **1992**, *114*, 5197.
(39) Bernhard, P.; Bürgi, H.-B.; Hauser, J.; Lehmann, H.; Ludi, A. *Inorg. Chem.* **1982**, *21*, 3936.

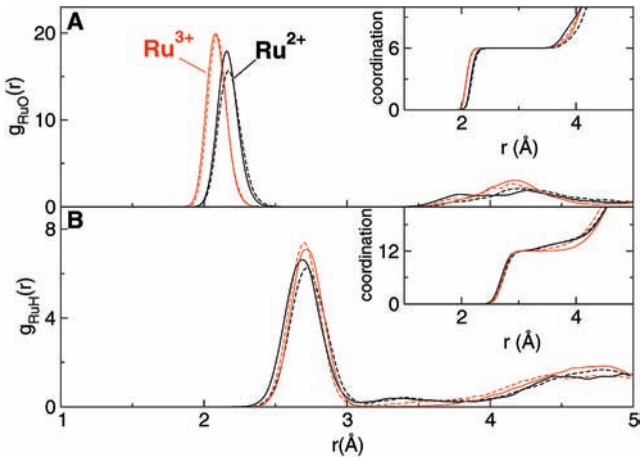

Figure 6. Radial distribution function $g(r)$ between the Ru atom of the solute, Ru(H$_2$O)$_6^{2+}$, and the O-atoms (A) and H-atoms (B) of water molecules (black). The corresponding radial distribution functions for Ru(H$_2$O)$_6^{3+}$ are shown in red. The coordination numbers obtained by spherical integration of the radial distributions are shown in the insets. (—) 1 Ru, 128 water molecules, PBE/DZVP, (- - -) 1 Ru, 32 water molecules, BLYP, plane wave basis, Car−Parrinello molecular dynamics, taken from ref 17. Data points were collected in bins of width 0.01 Å and the distributions were smoothed by convolution with a Gaussian of width 0.03 Å.

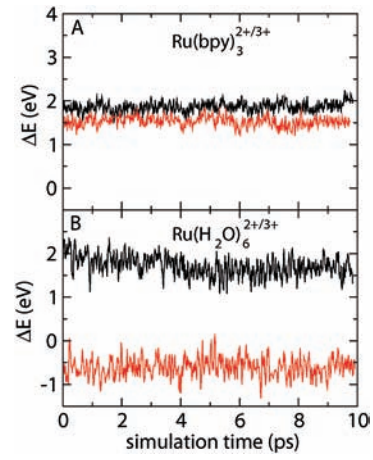

Figure 7. Fluctuation of the energy gap ΔE, eq 3, along density functional molecular dynamics trajectories of aqueous Ru(bpy)$_3^{2+}$ (A, black lines) and Ru(bpy)$_3^{3+}$ (A, red lines) and aqueous Ru(H$_2$O)$_6^{2+}$ (B, black lines) and Ru(H$_2$O)$_6^{3+}$ (B, red lines). The energy gap for the +2 ions correspond to ionization energies and the energy gap for the +3 ions to electron affinities. Note the large difference between ionization energy and electron affinity for the aquo complex but the small difference for the bipyridine complex.

oxidation states, amounting to 12 water molecules for the second coordination shell. The second minimum for Ru(H$_2$O)$_6^{2+}$ and Ru(H$_2$O)$_6^{3+}$ is at 4.96 and 4.74 Å indicating that both the first and the second solvation shells are closer packed in the oxidized state. While experimental information on the second coordination shell is not available for Ru ions, X-ray diffraction measurements of some di- and trivalent salts suggest that the second shell is comprised of about 12 water molecules in agreement with our finding.[40] This also confirms the computational model used in the mixed quantum-continuum study of ref 41.

4.2.2. Energy Gap Fluctuations. The fluctuations of the energy gap ΔE (eq 3) along DFMD trajectories of the Ru-complexes are shown in Figure 7. The energy gaps for the reduced ions (= ionization energies) are shown in black and the energy gaps for the oxidized ions (= electron affinity) in red. Properties calculated from the sampled energy gaps are summarized in Table 2. The rather short DFMD trajectories of length 10 ps are sufficiently long to converge the average energy gaps of Ru(bpy)$_3^{2+}$ and Ru(bpy)$_3^{3+}$ to a statistical uncertainty of 0.01 eV. The error is larger for Ru(H$_2$O)$_6^{2+}$ and Ru(H$_2$O)$_6^{3+}$, 0.06 and 0.02 eV, respectively. The widths of the fluctuations of Ru(bpy)$_3^{2+}$ and Ru(bpy)$_3^{3+}$ are identical within the statistical error, $\sigma_R = 0.10$ eV and $\sigma_O = 0.11$ eV, and similarly for Ru(H$_2$O)$_6^{2+}$ and Ru(H$_2$O)$_6^{3+}$, $\sigma_R = 0.22$ eV and $\sigma_O = 0.22$ eV, indicating that both ion pairs are in the linear response regime. This result is confirmed by the Gaussian shape of the probability distributions of the energy gap in reduced and oxidized states, see Figure 8 (where the shifted gap $\Delta E_\mu = \Delta E - \Delta A$ is displayed). The corresponding diabatic free energy profiles calculated according to eq 4 are also shown in Figure 8. They are well approximated by parabolic fit functions in accord with the prediction of linear response theory. The R^2 values for the parabolic fits are 0.9971 for Ru(bpy)$_3^{2+}$, 0.9963 for Ru(bpy)$_3^{3+}$, 0.9998 for Ru(H$_2$O)$_6^{2+}$, and 0.9997 for Ru(H$_2$O)$_6^{3+}$. Interestingly, the widths of the energy gap fluctuations of the bpy complexes are unusually small, just about half the value of the aquo complexes and other aqueous aquo-ions.[14,15] This is a consequence of the very rigid coordination of the Ru-ion by bpy ligands, giving rise to only a modest broadening of the HOMO level from where the electron is taken (illustrated in Figure 2). In contrast, the octahedral coordination structure of the Ru-aquo complex is much more dynamical giving rise to an increased broadening of the HOMO and the energy gap fluctuations, respectively. The average energy gap and the width of the gap fluctuations are subject to finite size effects that will be discussed in section 4.2.5.

Table 2. Redox Properties for Ru(bpy)$_3^{2+/3+}$ and Ru(H$_2$O)$_6^{2+/3+}$ in Aqueous Solution from Density Functional Molecular Dynamics Simulation[a]

	Ru(bpy)$_3^{2+/3+}$	Ru(H$_2$O)$_6^{2+/3+}$
$\langle\delta\Delta E^2\rangle_R^{1/2}$ [b]	0.10	0.22
$\langle\delta\Delta E^2\rangle_R^{1/2}$ [b]	0.11	0.22
ΔE_R [c]	1.86 ± 0.01	1.72 ± 0.06
ΔE_O [c]	1.53 ± 0.01	−0.61 ± 0.02
λ_R [d]	0.18 ± 0.05	1.20 ± 0.05
λ_O [d]	0.15 ± 0.05	1.13 ± 0.05
λ [e]	0.17 ± 0.01	1.16 ± 0.03
ΔA [f]	1.70 ± 0.01	0.55 ± 0.03

[a] See section 3 for simulation details. All energies are in eV. [b] Root-mean-square fluctuations of the energy gap, eq 3. [c] Equation 13. [d] Equations 6 and 7. [e] Equation 9. [f] Equation 12.

4.2.3. Reorganization Free Energy. The reorganization free energy λ_R (λ_O) is the free energy required to move the ions from the equilibrium configuration of diabatic state R (O) to the equilibrium configuration of diabatic state O (R) while staying on the same diabatic free energy surface of state R (O), see eqs 6−7. In the limit of linear response $\lambda = \lambda_R = \lambda_O$ with λ being equal to half of the difference of the mean energy gap in reduced and oxidized state, see eq 9. Comparing the reorganization free energies obtained from the parabolic fit functions in Figure 8, λ_R and λ_O, with the reorganization free energy λ calculated according to the linear response formula eq 9, we find that their numerical value coincides within the resolution (bin size) of the free energy profile, see Table 2. This further supports the

(40) Ohtaki, H.; Radnai, T. *Chem. Rev.* **1993**, *93*, 1157.
(41) Jaque, P.; Marenich, A. V.; Cramer, C. J.; Truhlar, D. G. *J. Phys. Chem. C* **2007**, *111*, 5783.

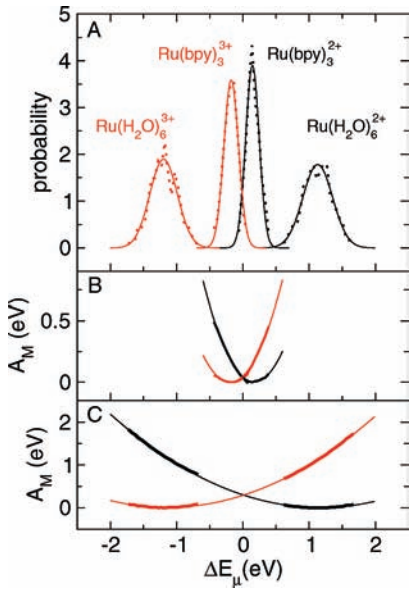

Figure 8. Probability distributions of the gap energy (A) and corresponding diabatic free energies (B),(C). The probability distribution depicted as dots was calculated according to eq 5 by collecting the gap energies shown in Figure 7 in bins of width 0.05 eV. The gap energies were then shifted by the oxidation free energy eq 12, $\Delta E_\mu = \Delta E - \Delta A$. Gaussian fit functions of the distributions are shown in solid lines. Data points for the diabatic free energy curves A_M, M = R, O, are shown in thick lines and parabolic fit functions in thin lines. The data points in the equilibrium region were obtained from the distributions shown in (A) according to eq 4. The data points at high free energies were obtained from the exact linear free energy relation $A_O - A_R = \Delta E$.[23] See ref 17 for a more detailed description for construction of the free energy curves.

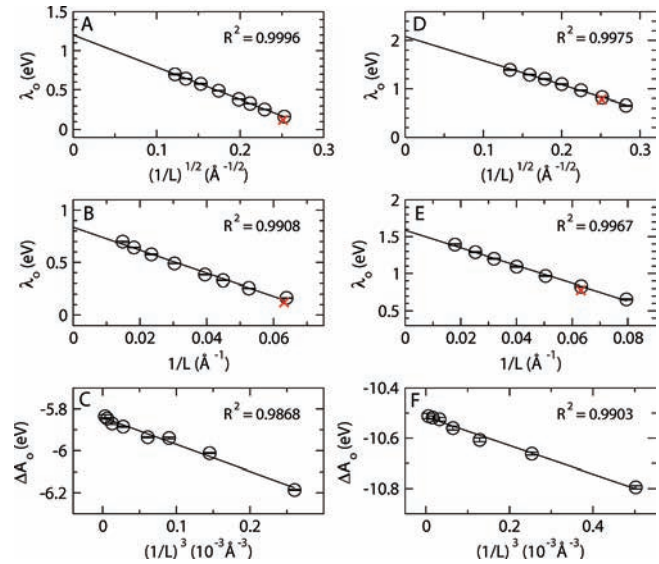

Figure 9. Dependence of the outer sphere reorganization free energy λ_o and oxidation free energy ΔA_o with respect to the length of the simulation cell, L. (A,B,C) is for oxidation of aqueous Ru(bpy)$_3^{2+}$ and (D,E,F) for oxidation of aqueous Ru(H$_2$O)$_6^{2+}$. Data points denoted by circles are fit to straight lines with a R^2 value as indicated. The statistical uncertainty due to the finite length of the simulation is indicated by error bars. The periodic systems contain one nonpolarizable solute molecule and a variable number of polarizable POL3 water[32] molecules per unit cell, see section 3 for details. The outer sphere contribution obtained from density functional molecular dynamics simulation of aqueous Ru(bpy)$_3^{2+/3+}$ and Ru(H$_2$O)$_6^{2+/3+}$ is denoted by a cross.

Table 3. Experimental (exp) and Computed Redox Properties of Aqueous Ru(bpy)$_3^{2+/3+}$ and Ru(H$_2$O)$_6^{2+/3+}$[a]

	Ru(bpy)$_3^{2+/3+}$		Ru(H$_2$O)$_6^{2+/3+}$
	exp[b]	DFMD[c]	DFMD[c]
λ	1.21 ± 0.04	(i) 1.20	2.42
		(ii) 0.84	1.92
σ	0.30 ± 0.04	(i) 0.25	0.35
		(ii) 0.21	0.32
ΔG^0	5.60	5.75	4.40
$\Delta\Delta G^0$	1.01	1.35	0
ΔE_R	6.81 ± 0.04	6.95	6.83

[a] Computed properties are obtained from density functional molecular dynamics (DFMD) simulation (see Table 2) and corrected for the finite size of the simulation cell and for the different zero potential energy reference relative to experiment. All energies are in eV. [b] $\lambda \equiv \lambda_O^b$, eq 1, $\Delta\kappa = 0$. $\sigma = 2^{-1}(2\ln 2)^{-1/2}$ fwhm with fwhm = 0.7 eV (HOMO). ΔG^0: absolute oxidation free enthalpy obtained from tabulated reduction potential versus normal hydrogen electrode (NHE, 1.24 V[1] for Ru(bpy)$_3^{2+/3+}$) and absolute oxidation free enthalpy of NHE (4.36 eV[35]). $\Delta\Delta G^0 = \Delta G^0$ (Ru(bpy)$_3^{2+/3+}$) − ΔG^0 (Ru(H$_2$O)$_6^{2+/3+}$). $\Delta E_R \equiv E_b$: binding energy of HOMO. [c] λ from Table 2 finite size corrected (i) according to the $1/L^{1/2}$ extrapolation (Figure 9A,D) and (ii) according to the $1/L$ extrapolation (Figure 9B,E). σ from eq 10. $\Delta G^0 \equiv \Delta A$ from Table 2 corrected for finite size according to the $1/L^3$ extrapolation (Figure 9C,F) and for the absolute potential shift (+3.7 eV). ΔE_R from Table 2 corrected by adding the finite size correction for λ (according to (i)) and ΔA and the absolute potential shift (+3.7 eV).

validity of the linear response approximation for the bpy and aquo complexes.

Before we compare computed with experimental reorganization free energy, we have to estimate a correction for the finite system size of the DFMD simulation. The reorganization free energy obtained is due to the solute and about 100 water molecules, but the contributions from higher solvation shells and bulk solvent is missing. Here we employ classical molecular dynamics simulation to estimate the missing solvent contribution. The reorganization free energy of the solvent ($= \lambda_o$) is computed for a series of systems with increasing number of polarizable water molecules (100 to 10 000 POL3 water molecules) and extrapolated to the limit of infinite dilution. Oxidation is modeled by removing point charges from the nonpolarizable solute molecule according to the difference in RESP charges in the reduced and oxidized state. The reorganization free energy is then calculated as in the quantum case (eq 9) replacing the quantum gap energy eq 3 by the electrostatic gap energy of the solvent (eq 7 in the SI).

The result of our finite size analysis is shown in Figure 9, numerical values are summarized in Table 1 in the SI. Best linear correlation for the bpy complex is obtained when λ_o is plotted against $1/L^{1/2}$, $R^2 = 0.9996$. The correlation for λ_o versus $1/L$ is still notable, $R^2 = 0.991$, but not as good. The choice for the best linear fit is not as clear for the aquo complex. For the fit against $1/L^{1/2}$ we obtain $R^2 = 0.9975$ and for the fit against $1/L$ $R^2 = 0.9967$. The finite size correction obtained as the difference in reorganization free energy at the intercept of the $1/L^{1/2}$ linear fit and the system size used in DFMD, is substantial, 1.04 eV for the bpy complex and 1.26 eV for the aquo complex. The total reorganization free energy of the infinitely diluted system is then estimated to be $\lambda = 0.17 + 1.04 = 1.20$ eV for the bpy complex and $\lambda = 1.16 + 1.26 = 2.42$ eV for the aquo complex. The computed estimate for the bpy complex is in excellent agreement with the experimental value of 1.21 eV (see Table 3 for a summary of experimental and computed results). However, the almost exact agreement with experiment should be considered with caution because of the uncertainty introduced by the extrapolation method. If the $1/L$ linear fit is used a total reorganization free energy of

0.84 eV is obtained for the bpy complex, 0.36 eV below the experimental estimate.

Irrespective of the method used for correction of finite system size, the reorganization free energy of the aquo complex is about 1 eV larger than for the bpy complex. A third of this difference can be related to the rigid coordination of the bpy complex. The change in Ru−N bond lengths upon oxidation of $Ru(bpy)_3^{2+}$ is just + 0.02 Å, whereas the change in Ru−O bond lengths upon oxidation of $Ru(H_2O)_6^{2+}$ is significantly larger, −0.08 Å (see Table 1). As a consequence of this, the inner sphere reorganization obtained from gas-phase calculations of the solute is significantly smaller for the bpy complex, $\lambda_i = 0.04$ eV, than for the aquo complex, $\lambda_i = 0.38$ eV, (calculations summarized in Table 2 in the SI). The remaining two-thirds of the difference is related to the reorganization of the outer sphere, and in particular to the large separation between the Ru-ion and the first solvation shell in the bpy complex. As discussed in section 4.2.1, the bpy ligands create a large hydrophobic cavity allowing only a few water molecules to approach the Ru ion at distances smaller than 6 Å (see Figures 2 and 5). For comparison, the full second solvation shell of the aquo complex comprised of 12 water molecules fits in a sphere of radius 5 Å (see Figure 6).

4.2.4. Redox Potential. The oxidation free energy corresponding to the redox potential of the aqueous ions is calculated according to eq 12. Since both ions are in the linear response regime (see section 4.2.2) eq 12 is essentially exact. Inserting the energy gaps obtained from DFMD simulation into eq 12 we obtain an oxidation free energy of $\Delta A = 1.70$ eV for $Ru(bpy)_3^{2+/3+}$ and 0.55 eV for $Ru(H_2O)_6^{2+/3+}$. Before we can compare these values to experiment we have to account for three systematic errors: (i) the finite size of the simulation cell, (ii) the different definition of the zero electrostatic potential reference in a periodic simulation cell and in experiment as we formally remove one electron from the system and (iii) possible deficiencies in the exchange-correlation functional used.

The finite size correction is obtained from the same classical simulations described before in section 4.2.3 by plotting ΔA_o against $1/L^3$, see Figure 9C,F. The $1/L^3$ plot gives the best linear correlation, $R^2 = 0.9868$ for the bpy and 0.9903 for the aquo complex. The difference between the intercept and the value for the system size used for DFMD gives a correction of 0.35 eV for the bpy complex and 0.15 eV for the aquo complex. The second correction term arises from the fact that in periodic boundary conditions the zero electrostatic potential reference is defined by $\int_{cell} d\mathbf{r}\phi(\mathbf{r}) = 0$ (ϕ being the Ewald potential),[42−46] whereas in experiment the zero potential reference is at an infinite distance away from the surface of the aqueous solution sample. Very recently, this difference in the absolute potential reference has been estimated by computation of the free energy for insertion of a proton in a periodic box of water and comparing to the experimental absolute hydration free energy.[47,48] This calculation carried out with the same periodic density functional molecular dynamics approach that is used herein, showed that the absolute cell potential for oxidation reactions is downshifted by 3.7 eV compared to experiment.[48] This shift, arising entirely from a different definition of the zero potential energy reference in simulation and experiment, has to be added to the computed ionization energies and redox potentials. Reorganization free energies remain unaffected by this shift because the net charge does not change during nuclear reorganization.

Adding the first two correction terms we obtain an oxidation free energy of $\Delta A = 1.70 + 0.35 + 3.7 = 5.75$ eV for $Ru(bpy)_3^{2+/3+}$ and $0.55 + 0.15 + 3.7 = 4.40$ eV for $Ru(H_2O)_6^{2+/3+}$, which places them within 0.2 eV of the experimental estimates, 5.60 and 4.59 eV, respectively. This error is comparable to the mean unsigned error of the PBE functional for the IP13 and EA14 databases for ionization potentials and electron affinities, 0.16 and 0.10 eV, respectively.[49] Indeed, calculations in the gas phase show that the adiabatic ionization free energy of $Ru(H_2O)_6^{2+}$ is about 0.4 eV smaller for PBE than for hybrid and hybrid meta-GGA functionals,[41] which partly explains the remaining deviation with experiment. For $Ru(bpy)_3^{2+/3+}$ the adiabatic ionization potential is less sensitive to the functional used. The values obtained with the PBE, BLYP and B3LYP exchange-correlation functionals are within 0.05 eV (see ΔE_i in Table 2 in the SI). We note that reorganization free energies are rather insensitive to the functional used for both, bpy and aquo complexes (see Table 2 in the SI).

Interestingly, the gas-phase ionization potential of $Ru(bpy)_3^{2+}$ is more than 3 eV *lower* than for $Ru(H_2O)_6^{2+}$, whereas the oxidation free energy (ie redox potential) of aqueous $Ru(bpy)_3^{2+}$ is 1 eV *higher* than for aqueous $Ru(H_2O)_6^{2+}$ (see Table 2 in the SI). Evidently, the stabilization of the oxidized state due to solvation is more than 4 eV larger for the aquo complex than for the bpy complex. The reason for this substantial difference is again related to the large hydrophobic cavity created by the bulky bpy ligands.

4.2.5. Vertical Ionization Energies. In experiment the binding energy is evaluated as $E_b = h\nu - KE$, that is, as the difference between excitation photon energy and the measured kinetic energy (KE) of the photoelectron ejected into vacuum. For the photon energies applied the photoemission process is instantaneous, occurring on the subfemtosecond time scale, and neglect of nuclear relaxation after electron removal is justified.[2,3] Furthermore, it seems adequate to assume that the final state is electronically relaxed as the measured gas−liquid shift of pure water does not change with photon energy.[2] Thus, for vanishing surface potential difference ($\Delta\kappa \approx 0$), the measured binding energy of the HOMO can be identified with the computed vertical ionization energy ΔE_R.

Again, before comparison to experiment is made we have to account for the finite system size of the simulation cell and the absolute potential shift in periodic boundary conditions. Since the vertical ionization energy is equal to the sum of oxidation free energy and reorganization free energy, the finite size correction for ΔE_R is just the sum of the two latter quantities, $1.04 + 0.35 = 1.39$ eV (using the $1/L^{1/2}$

(42) deLeeuw, S. W.; Perram, J. W.; Smith, E. R. *Proc. R. Soc. A* **1980**, *373*, 27.
(43) Kleinman, L. *Phys. Rev. B* **1981**, *24*, 7412.
(44) Asthagiri, D.; Pratt, L. R.; Ashbaugh, H. S. *J. Chem. Phys.* **2003**, *119*, 2702.
(45) Hunt, P.; Sprik, M. *Chem. Phys. Chem.* **2005**, *6*, 1805.
(46) Leung, K.; Marsman, M. *J. Chem. Phys.* **2007**, *127*, 154722.
(47) Sulpizi, M.; Sprik, M. *Phys. Chem. Chem. Phys.* **2008**, *10*, 5238.
(48) Adriaanse, C.; Sulpizi, M.; VandeVondele, J.; Sprik, M. *J. Am. Chem. Soc.* **2009**, *131*, 6046.
(49) Zhao, Y.; Truhlar, D. G. *J. Chem. Phys.* **2006**, *125*, 194101.

extrapolated value for λ). Adding this number and the absolute potential shift of 3.7 eV to the average ionization energy obtained from DFMD we obtain $\Delta E_R = 1.86 + 1.39 + 3.7 = 6.95$ eV for $Ru(bpy)_3^{2+}$. This value reproduces the experimental electron binding energy of 6.81 eV to within 0.2 eV. Interestingly, the computed number for $Ru(H_2O)_6^{2+}$, $\Delta E_R = 1.72 + 1.41 + 3.7 = 6.83$ eV, is very similar despite the lower oxidation free energy of the aquo complex (Table 3).

For the purpose of interpreting the experimental valence PE spectrum we turn from N and $N - 1$ electron energies (E_R, E_O) to one-electron Kohn−Sham (KS) orbital energies. This comparison is complicated by the fact that there is no formal correspondence between KS energies and experimental binding energies. There is one exception, though: the KS energy of the HOMO is equal to minus the vertical, electronically relaxed ionization energy,[50,51] $\Delta E = IP = -\varepsilon_{HOMO}$. However, this relation is rigorously valid only for the exact exchange-correlation functional. For approximate functionals the deviation can be substantial. This is the case in the present study. The thermal average of the KS-energy of the HOMO of $Ru(bpy)_3^{2+}$ is $\langle\varepsilon_{HOMO}\rangle_R = -1.19$ eV whereas the average ionization energy is $\Delta E_R = 1.86$ eV (finite size corrections and potential shift omitted).

It is with the above-mentioned caveats in mind that we compare the experimental PE spectrum with the computed KS density of states (DOS) shown in Figure 3. Aligning the computed and experimental peak of the $1b_1$ state of water at a binding energy (BE) of 11.16 eV by shifting the computed DOS by 7.67 eV, the computed peak positions for the $3a_1$, $1b_2$, and $2a_1$ bands are at a BE 13.96, 16.66, and 28.77 eV, respectively (note that BE is equal to minus the orbital energy). The computed peak positions are shifted by 0.46, −0.68, and −2.13 eV relative to the experimental peak positions. Similar results and deviations have been reported previously for pure liquid water[52] indicating that the solute has only a marginal effect on the occupied states of water in agreement with experiment (see section 4.1). In the spectrum aligned wrt the $1b_1$ peak the computed position of the peak of the HOMO level of $Ru(bpy)_3^{2+}$ is at a too high BE, 9.16 eV, compared with the experimental peak position at 6.81 eV. Thus, the orbital energy gap between the center of the $1b_1$ band and the center of the peak of the HOMO of $Ru(bpy)_3^{2+}$ is underestimated by more than 2 eV.

While the agreement between computed DOS and experimental PES is only qualitatively correct, we expect that the calculations provide helpful insight into the assignment of electronic states. In Figure 10 we show the fluctuations of occupied and empty KS-energy levels of aqueous $Ru(bpy)_3^{2+}$ along a DFMD trajectory. The computed levels are again aligned wrt the experimental $1b_1$ band of water. Occupied and empty solute states are inserted into the band gap of liquid water. The lowest solute states are composed of π orbitals of the bpy ligands. They are clearly separated from the three d-orbitals of t_{2g} character located on the metal ion. The LUMO and the following eight empty states are composed of π^* orbitals of the ligands. They are inserted into the gap between the occupied t_{2g} and the lowest unoccupied d orbital of the metal ($d_{x^2-y^2}$ character). Another four π^* orbitals are inserted into the gap between the latter and the highest unoccupied d orbital of the metal (d_{z^2} character). All levels higher in energy form the conduction band of liquid water.

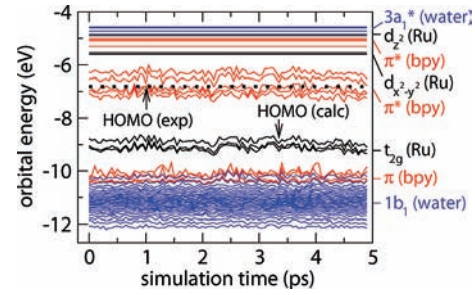

Figure 10. Kohn−Sham orbital energies along a density functional molecular dynamics trajectory of aqueous $Ru(bpy)_3^{2+}$. The energy levels are shifted so as to align the $1b_1$ peak of the experimental PE spectrum with the one of the computed density of states. The Kohn−Sham energies are equal to minus the binding energies shown in Figure 3. The center of the experimental peak for the HOMO level at −6.81 eV is indicated by a dotted line. The assignment of the levels is based on visual inspection of the orbitals. For the $1b_1$ water band every fifth Kohn−Sham energy level is drawn. For states $d_{x^2-y^2}$ to $3a_1^*$ the energy of the last snapshot is displayed, only.

5. Conclusion and Outlook

To summarize, we have presented the energy resolved PE spectrum of aqueous $Ru(bpy)_3^{2+}$ and determined an experimental value for the reorganization free energy of $Ru(bpy)_3^{3+}$. Using density functional MD simulations and correcting for the finite size of the simulation cell and the absolute potential shift, we could reproduce the experimental electron binding energy, redox potential and reorganization free energy fairly well. Subsequent calculations for the $Ru(H_2O)_6^{2+/3+}$ redox pair gave a similar electron binding energy but a reorganization free energy that was significantly larger, by $\Delta\lambda_O = \lambda_O(aquo) - \lambda_O(bpy) = 1.1-1.2$ eV. Analysis of the coordination geometry and solvation structure revealed that the large reorganization free energy of $Ru(H_2O)_6^{2+/3+}$ is due to increased inner-sphere reorganization (about one-third of the difference) and due to increased outer sphere reorganization (about two-third of the difference).

We finally return to the question posed in the introduction regarding the large difference in redox potential between $Ru(bpy)_3^{2+/3+}$ and $Ru(H_2O)_6^{2+/3+}$. Adopting the picture in Figure 1 the difference in oxidation free energy is $\Delta\Delta G^0 = \Delta G^0(aquo) - \Delta G^0(bpy) = \Delta\Delta E_R - \Delta\lambda_O = -1.01$ eV. Comparing $\Delta\Delta G^0 = -1.01$ eV with $\Delta\lambda_O = 1.1-1.2$ eV we find that the difference in redox potential is mainly associated with the higher reorganization free energy of the aquo complex compared to the bpy complex. This implies that the difference in vertical ionization energy ($\Delta\Delta E_R$) is minor and that the experimental binding energy of the HOMO of $Ru(H_2O)_6^{2+}$ is close to the one obtained for $Ru(bpy)_3^{2+}$. It would be interesting to verify this prediction in future PE experiments.

In this work we have shown that DFMD is a promising method for quantitative estimation of single-ion reorganization free energies, electron binding energies and redox potentials provided that the results are corrected for finite system size, and the latter two quantities for the different definition of the zero potential reference in periodic simula-

(50) Almbladh, C. O.; von Barth, U. *Phys. Rev. B* **1985**, *31*, 3231.
(51) Chong, D. P.; Gritsenko, O. V.; Baerends, E. J. *J. Chem. Phys.* **2002**, *116*, 1760.
(52) Hunt, P.; Sprik, M.; Vuilleumier, R. *Chem. Phys. Lett.* **2003**, *376*, 68.
(53) Brunschwig, B. S.; Creutz, C.; McCartney, D. H.; Sham, T.-K.; Sutin, N. *Faraday Discuss. Chem. Soc.* **1982**, *74*, 113.

tions and in experiment. We would like to corroborate this view in future work by comparing computed and experimental redox properties of a number of aqueous transition metal complexes that are amenable to energy resolved PE measurements.

Acknowledgment. R.S., M.F., and B.W. thank the staff of BESSY for assistance. J.B. acknowledges helpful discussions with Prof. M. Sprik, The Royal Society for a University Research Fellowship and a research grant, and the HPC Facility "Darwin" at the University of Cambridge for generous computer time.

Supporting Information Available: Description of two, more approximate and computationally less expensive approaches for calculation of reorganization free energy (QM+MM and continuum calculations) and further details for finite system size correction; 3 tables summarizing finite system size correction, gas phase calculations of the solutes, and redox properties comparing DFMD, QM+MM and continuum calculations; the complete refs 28 and 31. This material is available free of charge via the Internet at http://pubs.acs.org.

JA9047834